

Timelike geodesics in three-dimensional rotating Hořava AdS black hole

P. A. González*

*Facultad de Ingeniería y Ciencias, Universidad Diego Portales,
Avenida Ejército Libertador 441, Casilla 298-V, Santiago, Chile*

Marco Olivares†

*Facultad de Ingeniería y Ciencias, Universidad Diego Portales,
Avenida Ejército Libertador 441, Casilla 298-V, Santiago, Chile*

Eleftherios Papantonopoulos‡

*Department of Physics, National Technical University of Athens,
Zografou Campus GR 157 73, Athens, Greece*

Yerko Vásquez§

*Departamento de Física, Facultad de Ciencias, Universidad de La Serena,
Avenida Cisternas 1200, La Serena, Chile* (Received 8 August 2020; accepted 29 March 2021; published 21 April 2021)

We study the motion of particles in the background of a three-dimensional rotating Hořava anti–de Sitter black hole that corresponds to a Lorentz-violating version of the Bañados-Teitelboim-Zanelli (BTZ) black hole and we analyze the effect of the breaking of Lorentz invariance in such motion by solving analytically the geodesic equations. Mainly, we find that the Lorentz-violating version of the BTZ black hole possesses a more rich geodesic structure, where the planetary and circular orbits are allowed, which does not occur in the BTZ background.

DOI: [10.1103/PhysRevD.103.084037](https://doi.org/10.1103/PhysRevD.103.084037)**I. INTRODUCTION**

The three-dimensional models of gravity are of interest because it is possible to investigate efficiently some of their properties that are shared by their higher-dimensional analogs and also exhibit interesting solutions such as particlelike solutions and black holes. In this context, three-dimensional general relativity (GR), which has no local gravitational degrees of freedom and is Lorentz invariant, presents the well-known Bañados-Teitelboim-Zanelli (BTZ) black hole solution with a negative cosmological constant [1]. Also, it presents interesting properties at both classical and quantum levels and the BTZ solution shares several features of the Kerr black hole [2]. An important issue in gravitational physics is to know the kind of orbits that test particles follow outside the event horizon of a black hole. This information can be provided by studying the geodesics around these black holes; in this context, for the BTZ background, it was shown that, while massive particles always fall into the event horizon and no

stable orbits are possible [3], massless particles can escape or plunge to the horizon [4].

The three-dimensional Hořava gravity [5] admits a Lorentz-violating version of the BTZ black hole, i.e., a black hole solution with anti–de Sitter (AdS) asymptotics, only in the sector of the theory in which the scalar degree of freedom propagates infinitely fast [6]. Remarkably, in contrast to GR, the three-dimensional Hořava gravity also admits black holes with positive and vanishing cosmological constant. Nowadays, one could think that Lorentz invariance may not be fundamental or exact, but is merely an emergent symmetry on sufficiently large distances or low energies. It has been suggested in Ref. [7] that giving up Lorentz invariance by introducing a preferred foliation and terms that contain higher-order spatial derivatives can lead to significantly improved UV behavior; the corresponding gravity theory is dubbed Hořava gravity. It was shown that the propagation of massive scalar fields is stable in the background of rotating three-dimensional Hořava AdS black holes and, by employing the holographic principle, the different relaxation times of the perturbed system to reach thermal equilibrium were found for the various branches of solutions [8]. Also, it was shown that particles can collide on the inner horizon with arbitrarily high c.m. energy if one of the particles has a critical angular

* pablo.gonzalez@udp.cl

† marco.olivaresr@mail.udp.cl

‡ lpapa@central.ntua.gr

§ yvasquez@userena.cl

momentum being possible the Bañados-Silk-West process, for the nonextremal rotating Hořava AdS black hole. Also, while for the extremal BTZ black hole the particles with critical angular momentum only can exist on the degenerate horizon, for the Lorentz-violating version of the BTZ black hole, the particle with critical angular momentum can exist in a region from the degenerate horizon [9]. Concerning the null geodesics, it was shown that for the motion of photons new kinds of orbits are allowed, such as unstable circular orbits and trajectories of the first kind. Also, it was shown that an external observer will see that photons arrive at spatial infinity in a finite coordinate time [10].

In this work we study the motion of particles in the background of a three-dimensional rotating Hořava AdS black hole [6], with the aim of analyzing the effect of breaking the Lorentz symmetry by calculating the timelike geodesic structure. We will show that Lorentz-violating version of the BTZ black hole possesses a more rich geodesic structure, where the planetary orbits are allowed, which does not occur in the BTZ background. Also, we will have a complete knowledge of the geodesic structure for the rotating three-dimensional Hořava AdS black hole, allowing us to understand in depth the Lorentz-violating effects on the BTZ black hole. For other studies about geodesics in three-dimensional spacetimes, see [11–14].

The work is organized as follows. In Sec. II, we give a brief review of a three-dimensional rotating Hořava AdS black hole. In Sec. III, we find the motion equations for particles, and we present the timelike geodesic structure in Sec. IV. Finally, our conclusions are in Sec. V.

II. THREE-DIMENSIONAL ROTATING HOŘAVA BLACK HOLES

The three-dimensional Hořava gravity is described in a preferred foliation by the action [5]

$$S_H = \frac{1}{16\pi G_H} \int dT d^2x N \sqrt{g} [L_2 + L_4], \quad (1)$$

being the line element in the preferred foliation

$$ds^2 = N^2 dT^2 - g_{ij}(dx^i + N^i dT)(dx^j + N^j dT), \quad (2)$$

where g_{ij} is the induced metric on the constant- T hypersurfaces. G_H is a coupling constant with dimensions of a length squared, g is the determinant of g_{ij} , and the Lagrangian L_2 has the following form:

$$L_2 = K_{ij}K^{ij} - \lambda K^2 + \xi({}^{(2)}R - 2\Lambda) + \eta a_i a^i, \quad (3)$$

where K_{ij} , K , and ${}^{(2)}R$ correspond to extrinsic, mean, and scalar curvature, respectively, and a_i is a parameter related to the lapse function N via $a_i = -\partial_i \ln N$. L_4 corresponds to the set of all the terms with four spatial derivatives that

are invariant under diffeomorphisms. For $\lambda = \xi = 1$ and $\eta = 0$, the action reduces to that of general relativity. In the infrared limit of the theory, the higher-order terms L_4 (UV regime) can be neglected, and the theory is equivalent to a restricted version of the Einstein-aether theory, the equivalence can be showed by restricting the aether to be hypersurface orthogonal and the following relation is obtained:

$$u_\alpha = \frac{\partial_\alpha T}{\sqrt{g^{\mu\nu} \partial_\mu T \partial_\nu T}}, \quad (4)$$

where u_α is a unit-norm vector field called the aether, see Ref. [15] for details. Another important characteristic of this theory is that only in the sector $\eta = 0$, Hořava gravity admits asymptotically AdS solutions [6]. Therefore, assuming stationary and circular symmetry, the most general metric is given by

$$ds^2 = Z(r)^2 dt^2 - \frac{1}{F(r)^2} dr^2 - r^2(d\phi + \Omega(r)dt)^2, \quad (5)$$

and by assuming the aether to be hypersurface orthogonal, it results in

$$u_t = \pm \sqrt{Z(r)^2(1 + F^2(r)U^2(r))}, \quad u_r = U(r). \quad (6)$$

The theory admits the BTZ “analog” to the three-dimensional rotating Hořava black holes described by the solution

$$F(r)^2 = Z(r)^2 = -M + \frac{\bar{J}^2}{4r^2} - \bar{\Lambda}r^2, \quad \Omega(r) = -\frac{J}{2r^2},$$

$$U(r) = \frac{1}{F(r)} \left(\frac{a}{r} + br \right), \quad (7)$$

where

$$\bar{J}^2 = \frac{J^2 + 4a^2(1 - \xi)}{\xi}, \quad \bar{\Lambda} = \Lambda - \frac{b^2(2\lambda - \xi - 1)}{\xi}. \quad (8)$$

The sign of the effective cosmological constant $\bar{\Lambda}$ determines the asymptotic behavior (flat, de Sitter, or AdS) of the metric. Also, \bar{J}^2 can be negative; this occurs when either $\xi < 0$ or $\xi > 1$, $a^2 > J^2/(4(\xi - 1))$. The aether configuration for this metric is given explicitly by

$$u_t = \sqrt{F^2 + \left(\frac{a}{r} + br \right)^2},$$

$$u_r = \frac{1}{F^2} \left(\frac{a}{r} + br \right), \quad u_\phi = 0, \quad (9)$$

where a and b are constants that can be regarded as measures of aether misalignment, with b as a measure of

asymptotically misalignment, such that for $b \neq 0$ the aether does not align with the timelike Killing vector asymptotically. Note that for $\xi = 1$ and $\lambda = 1$, the solution becomes the BTZ black hole, and for $\xi = 1$ and $\lambda \neq 1$, the solution becomes the BTZ black hole with a shifted cosmological constant $\bar{\Lambda} = \Lambda - 2b^2(\lambda - 1)$. However, there is still a preferred direction represented by the aether vector field that breaks Lorentz invariance for $\lambda \neq 1$ and $b \neq 0$. The locations of the inner and outer horizons $r = r_{\pm}$, are given by

$$r_{\pm}^2 = -\frac{M}{2\bar{\Lambda}} \left(1 \pm \sqrt{1 + \frac{\bar{J}^2 \bar{\Lambda}}{M^2}} \right). \quad (10)$$

Considering $M > 0$, a negative cosmological constant $\bar{\Lambda} < 0$, and $\bar{J}^2 > 0$, the condition $-\bar{J}^2 \bar{\Lambda} \leq M^2$ must be fulfilled for the solution represents a black hole. For $0 < -\bar{J}^2 \bar{\Lambda} < M^2$, the black holes have inner and outer horizons r_- and r_+ , the extremal case corresponds to $-\bar{J}^2 \bar{\Lambda} = M^2$, while that for $\bar{J}^2 < 0$ the black holes have outer horizon r_+ , but no inner horizon r_- .

Besides the existence of inner and outer horizons, also there are universal horizons, which are given by [6]

$$(r_u^{\pm})^2 = \frac{M - 2ab}{2(b^2 - \bar{\Lambda})} \pm \frac{1}{2(b^2 - \bar{\Lambda})} [(M - 2ab)^2 - (4a^2 + \bar{J}^2)(b^2 - \bar{\Lambda})]^{\frac{1}{2}}. \quad (11)$$

On the other hand, the existence of a well-defined spacelike foliation is essential in Hořava gravity. As it was shown in Ref. [6], this can be achieved by imposing the condition $F^2 + (a/r + br)^2 > 0$ or

$$\frac{1}{r^2} \left((b^2 - \bar{\Lambda})r^4 + (2ab - M)r^2 + \left(\frac{\bar{J}}{4} + a^2 \right) \right) > 0. \quad (12)$$

Figure 1 shows the behavior of the horizons as a function of the parameter b and as a function of a in Fig. 2 for a choice of parameters. There are different zones: one of them is limited by r_- and r_+ , and it is described by the existence of the aether, where the roots r_u^{\pm} are imaginary and therefore there are no universal horizons. Other zones are characterized by two real and distinct universal horizons inside the region between r_- and r_+ , outside r_- , and inside r_+ ; and an especial zone where both universal horizons coincide and given by

$$r_u^2 = \frac{M - 2a_{\pm}(M, \bar{J}, b)b}{2(b^2 - \bar{\Lambda}(b))}, \quad (13)$$

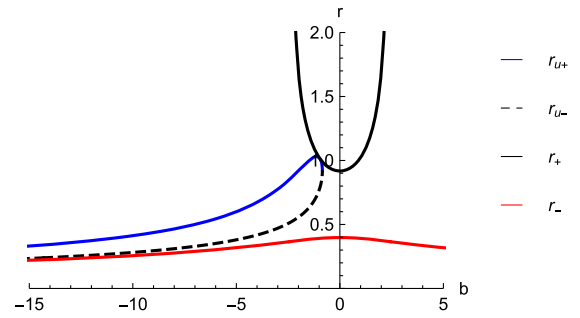


FIG. 1. The behavior of the horizons as a function of parameter b , with $M = 1$, $\xi = 1.2$, $\lambda = 1$, $a = 1$, $\Lambda = -1$, and $J = 1.2$. For $b \approx -0.84$, $r_u^+ = r_u^-$ [9].

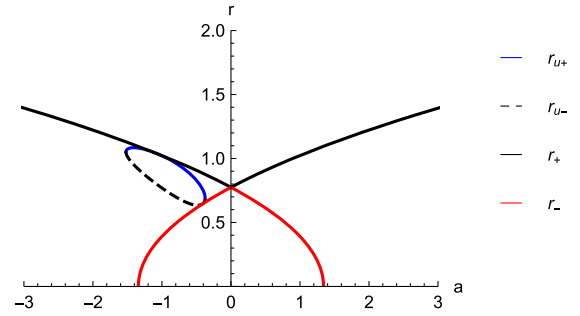


FIG. 2. The behavior of the horizons as a function of parameter a , with $M = 1$, $\xi = 1.2$, $\lambda = 1$, $b = 1$, $\Lambda = -1$, and $J = 1.2$. For $a \approx -1.52$ and -0.37 , $r_u^+ = r_u^-$ [9].

where a_{\pm} are the roots of

$$\frac{(4a^2 + \bar{J}^2)(b^2 - \bar{\Lambda}(b))}{\xi(M - 2ab)^2} = 1. \quad (14)$$

In the region between r_u^- and r_u^+ , the aether turns imaginary and the foliation cannot be extended until the singularity.

In order to analyze the roots of the lapse function, the case $J = 0$, we will consider a set of values for the parameters that satisfied the existence of two horizons r_- and r_+ , so the condition $0 < -\bar{J}^2 \bar{\Lambda} < M^2$ must be satisfied, and also there are not universal horizons; thereby the roots of r_u^{\pm} are imaginary, as in our previous analysis. So, in order to satisfy the above condition, the parameter ξ must satisfied $\xi_e < \xi < \xi_c$, where ξ_e corresponds to the value of ξ for which the black hole is extremal

$$\xi_e = \frac{2a^2(\sqrt{a^2(\Lambda - 2b^2(\lambda - 1))^2 + b^2(2\lambda - 1)M^2 - 2b^2\lambda - \Lambda})}{M^2 - 4a^2(b^2 + \Lambda)}, \quad (15)$$

and ξ_c is the value of ξ for which the black hole passes from having two horizons to having one horizon and it is $\xi_c = 1$ for nonrotating black holes. For $\xi > \xi_c$ the black holes are

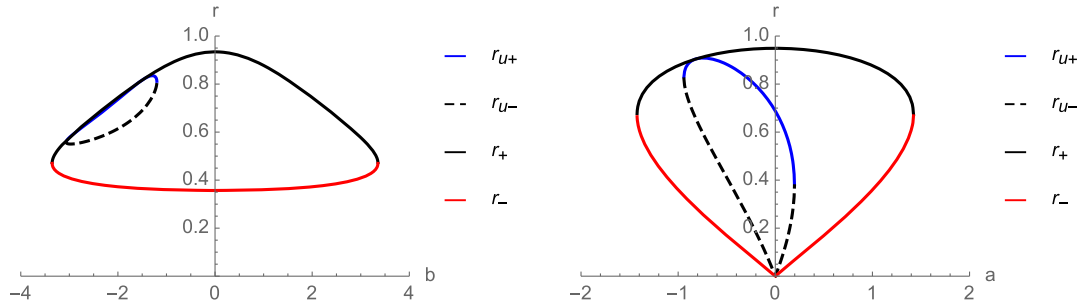


FIG. 3. The behavior of the horizons for nonrotating black holes as a function of the parameter b (left) with $a = 1$ and as a function of the parameter a (right) with $b = 1$. Here, $M = 1$, $\xi = 0.9$, $\lambda = 1$, and $\Lambda = -1$.

described by one horizon [8]. In Fig. 3, we plot the behavior of the horizons for $\xi = 0.9$ for nonrotating black holes.

In the following, we will focus mainly on a set of values for the parameters that satisfied the existence of two horizons r_- and r_+ , with $a > 0$ and $b > 0$, where there are not universal horizons; thereby the roots of r_u^\pm are imaginary, see Figs. 1–3. Note that under the conditions $M > 0$, $\bar{J}^2 > 0$, and $\bar{\Lambda} < 0$, the roots of r_u^\pm are imaginary when $M < 2ab$ from Eq. (11).

III. EQUATIONS OF MOTION

In this section, we find the motion equations of test massive particles around the three-dimensional Hořava AdS black hole. It is important to emphasize [16] that, in a Lorentz-violating scenario, particles will be generically coupled to the aether field, generating UV modifications of the matter dispersion relations; furthermore, one can also expect radiative corrections in the infrared sector, but these contributions are suppressed by known mechanisms. In our analysis we are interested in the infrared limit of the theory; so the presence of higher-order terms (L_4) related to the UV behavior of the theory is ignored and in this case the theory can be formulated in a covariant fashion. It then becomes equivalent to a restricted version of Einstein-aether theory [6]. Since our analysis is focused on the low energy part of the theory, the interaction between the massive particle and the aether field is ignored; thus the presence of the aether field only affects the background spacetime geometry. It is worth mentioning that a similar analysis was performed in [17] where the authors analyzed the evolution of the photon around the static neutral and charged aether black holes using the Hamilton-Jacobi equation. Therefore, the massive particles follow the typical geodesics in such given black holes spacetime that can be derived from the Lagrangian of a test particle, which is given by [18]

$$\mathcal{L} = \frac{1}{2} \left(g_{\mu\nu} \frac{dx^\mu}{d\tau} \frac{dx^\nu}{d\tau} \right). \quad (16)$$

So, for the three-dimensional rotating Hořava AdS black hole described by the metric (5), the Lagrangian associated with the motion of the test particles is given by

$$2\mathcal{L} = -[\mathcal{F}(r) - r^2\Omega^2(r)]\dot{t}^2 + 2r^2\Omega(r)\dot{t}\dot{\phi} + \frac{\dot{r}^2}{\mathcal{F}(r)} + r^2\dot{\phi}^2, \quad (17)$$

where $\dot{q} = dq/d\tau$, and τ is an affine parameter along the geodesic. Here, we have defined $F(r)^2 = Z(r)^2 = \mathcal{F}(r)$. Since the Lagrangian (17) is independent of the cyclic coordinates (t, ϕ) , then their conjugate momenta (Π_t, Π_ϕ) are conserved. Then, the equations of motion are obtained from $\dot{\Pi}_q - \frac{\partial \mathcal{L}}{\partial q} = 0$ and yield

$$\begin{aligned} \dot{\Pi}_t &= 0, \\ \dot{\Pi}_r &= -[\mathcal{F}'(r)/2 - r\Omega^2(r) - r^2\Omega'(r)]\dot{t}^2 - \frac{\mathcal{F}'(r)\dot{r}^2}{2\mathcal{F}^2(r)} + r\dot{\phi}^2, \\ \text{and } \dot{\Pi}_\phi &= 0, \end{aligned} \quad (18)$$

where $\Pi_q = \partial \mathcal{L} / \partial \dot{q}$ are the conjugate momenta to the coordinate q and are given by

$$\begin{aligned} \Pi_t &= -[\mathcal{F}(r) - r^2\Omega^2(r)]\dot{t} + r^2\Omega(r)\dot{\phi} \equiv -E, \\ \Pi_r &= \frac{\dot{r}}{\mathcal{F}(r)}, \quad \text{and} \quad \Pi_\phi = r^2\Omega(r)\dot{t} + r^2\dot{\phi} \equiv L, \end{aligned} \quad (19)$$

where E and L are integration constants associated with each of them. Therefore, the Hamiltonian is given by

$$\mathcal{H} = \Pi_t \dot{t} + \Pi_\phi \dot{\phi} + \Pi_r \dot{r} - \mathcal{L}. \quad (20)$$

Thus,

$$2\mathcal{H} = -E\dot{t} + L\dot{\phi} + \frac{\dot{r}}{\mathcal{F}(r)} \equiv -m^2, \quad (21)$$

where $m = 1$ for timelike geodesics or $m = 0$ for null geodesics. Therefore, we obtain

$$\dot{\phi} = -\frac{1}{(r^2 - r_+^2)(r^2 - r_-^2)\bar{\Lambda}} \left[\frac{EJ}{2} + L \left(-\bar{\Lambda}r^2 - M - \frac{J^2 - \bar{J}^2}{4r^2} \right) \right], \quad (22)$$

$$\dot{t} = -\frac{[Er^2 - JL/2]}{(r^2 - r_+^2)(r^2 - r_-^2)\bar{\Lambda}}, \quad (23)$$

$$\begin{aligned} i^2 &= \left(E - \frac{JL}{2r^2}\right)^2 - \left(-M + \frac{\bar{J}^2}{4r^2} - \bar{\Lambda}r^2\right)\left(m^2 + \frac{L^2}{r^2}\right) \\ &= (E - V_-)(E - V_+), \end{aligned} \quad (24)$$

where $V_{\pm}(r)$ is the effective potential and is given by

$$V_{\pm}(r) = \frac{JL}{2r^2} \pm \sqrt{\left(-M + \frac{\bar{J}^2}{4r^2} - \bar{\Lambda}r^2\right)\left(m^2 + \frac{L^2}{r^2}\right)}. \quad (25)$$

Since the negative branches have no classical interpretation, they are associated with antiparticles in the framework of quantum field theory [19]. We choose the positive branch of the effective potential $V = V_+$. In the next section, we will perform a general analysis of the equations of motion. Note that if $\dot{t} > 0$ for all $r > r_+$, the motion is forward in time outside the horizon; so from Eq. (23) for $\bar{\Lambda} < 0$ the following condition must be fulfilled:

$$Er^2 - JL/2 > 0. \quad (26)$$

On the other hand, Eq. (22) can be rewritten as

$$\dot{\phi} = -\frac{1}{(r^2 - r_+^2)(r^2 - r_-^2)\bar{\Lambda}} \left[\frac{J}{2r^2} \left(Er^2 - \frac{JL}{2} \right) + LF(r)^2 \right], \quad (27)$$

due to the term $Er^2 - JL/2 > 0$ and $F(r)^2 > 0$ for $r > r_+$; when L and J have the same sign ($JL > 0$), the term in square brackets does not have zeros outside the event horizon. However, when L and J have different signs ($JL < 0$), the zeros can be in the relevant domain, and it

would not necessarily indicate a turning point. In fact, the positive root (R) of the term in square brackets in Eq. (22) is

$$R^2 = \frac{JE}{4\bar{\Lambda}L} - \frac{M}{2\bar{\Lambda}} - \frac{\sqrt{(4LM - 2JE)^2 - 16\bar{\Lambda}L(J^2L - \bar{J}^2L)}}{8\bar{\Lambda}L}, \quad (28)$$

and it corresponds to the point where the angular velocity of the test particle $\omega(r)$,

$$\dot{\phi}/\dot{t} = \frac{d\phi}{dt} = \frac{\frac{EJ}{2} + L(-\bar{\Lambda}r^2 - M - \frac{J^2 - \bar{J}^2}{4r^2})}{Er^2 - JL/2} \equiv \omega(r), \quad (29)$$

is null. Also note that, for a motion with $L = 0$, $\omega(r) = \frac{J}{2r^2}$. Thus, a particle dropped ‘‘straight in’’ ($L = 0$) from a finite distance is ‘‘dragged’’ just by the influence of gravity, so that it acquires an angular velocity (ω) in the same sense as that of the source of the metric (J); this effect is called ‘‘dragging of inertial frames.’’

IV. TIMELIKE GEODESICS

In this section, we analyze the motion of particles, $m^2 = 1$, so the effective potential is given by

$$V(r) = \frac{JL}{2r^2} + \sqrt{\left(-M + \frac{\bar{J}^2}{4r^2} - \bar{\Lambda}r^2\right)\left(1 + \frac{L^2}{r^2}\right)}, \quad (30)$$

whose behavior is shown in Fig. 4 for $J > 0$ and positive values of the angular momentum of the particle (direct geodesics) and for $J < 0$ and positive values of the angular momentum of the particle (retrograde geodesics). We can observe for direct geodesics (Fig. 4, left) there is a critical value of the angular momentum (L_{LSCO}) where the last stable circular orbit (LSCO) is present at $r = r_{\text{LSCO}}$; and for $L > L_{\text{LSCO}}$ we can distinguish four orbits: the planetary,

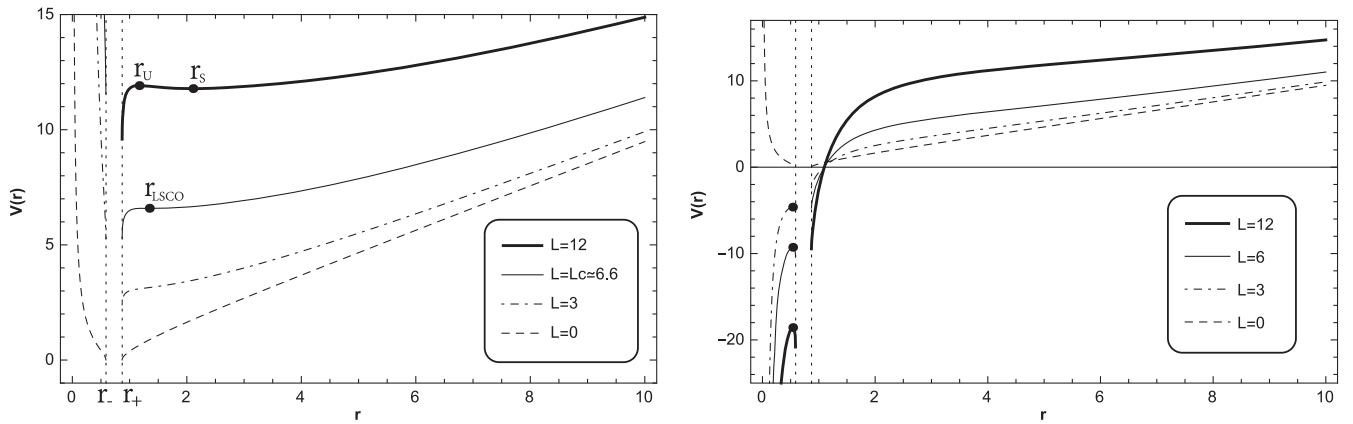


FIG. 4. The behavior of $V(r)$ as a function of r , for different values of the angular momentum of the particle L , with $M = a = b = \lambda = 1$, $\xi = 1.1$, $r_+ \approx 0.87$, and $\Lambda = -1$. Left: direct geodesics with $J = 1.2$. Right: retrograde geodesics with $J = -1.2$. The points (right) indicate the extreme value of the potentials that are located at $r_{\text{ext}} < r_+$.

second kind, circular unstable at $r = r_U$, and circular stable at $r = r_S$, and critical orbits are allowed. We will study the existence of circular orbit in detail in Sec. IV B. Note that the BTZ background is allowed orbits of second kind. So, the spacetime analyzed presents a richer geodesic structure. Also, for retrograde geodesics (Fig. 4, right) we can observe that, for $r > r_+$, circular and planetary orbits are not allowed. Here, the trajectory always has a turning point, from which the particle plunges in the event horizon, known as the trajectory of second kind.

The orbit in polar coordinates is given by [20]

$$-\frac{r^2}{(r^2 - r_+^2)(r^2 - r_-^2)\bar{\Lambda}} \left[\frac{EJ}{2} + L \left(-\bar{\Lambda}r^2 - M - \frac{J^2 - \bar{J}^2}{4r^2} \right) \right] \times \left(\pm \frac{dr}{d\phi} \right) = \sqrt{P(r)}, \quad (31)$$

where we have used Eqs. (22) and (24), $P(r)$ corresponds to the characteristic polynomial, and it is given by

$$P(r) = r^6 \bar{\Lambda} + r^4 (E^2 + L^2 \bar{\Lambda} + M) + r^2 (L^2 M - JEL - \bar{J}^2/4) + (J^2 - \bar{J}^2)L^2/4, \\ P(r) \equiv -\bar{\Lambda}(-r^6 + \alpha r^4 + \beta r^2 + \gamma), \quad (32)$$

where

$$\alpha = -\frac{E^2 + M + \bar{\Lambda}L^2}{\bar{\Lambda}}, \quad (33)$$

$$\beta = \frac{JEL + \bar{J}^2/4 - ML^2}{\bar{\Lambda}}, \quad (34)$$

$$\gamma = -\frac{(J^2 - \bar{J}^2)L^2}{4\bar{\Lambda}}. \quad (35)$$

Therefore, we can see that depending on the nature of its roots, we can obtain the allowed motions for this spacetime.

A. Planetary orbit

The roots of $P(r) = 0$ allows us to define the distance r_P , which corresponds to a “periastron” distance at the trajectory r_A , which is interpreted as an “apoastron” distance, and the distance r_F that represents the turning point for the trajectory, see Fig. 5. Thereby, planetary orbits of the first kind occur when $L > L_C$, and the energy E lies in the range $E_S < E < E_U$, so the radial coordinate will be $r_P < r < r_A$ for a certain value of E ; the planetary orbits of the second kind occur when $E < E_U$ and $r_H < r < r_F$.

Thus, the characteristic polynomial (32) can be written as

$$P(r) = -\bar{\Lambda}(r_A^2 - r^2)(r^2 - r_P^2)(r^2 - r_F^2), \quad (36)$$

where

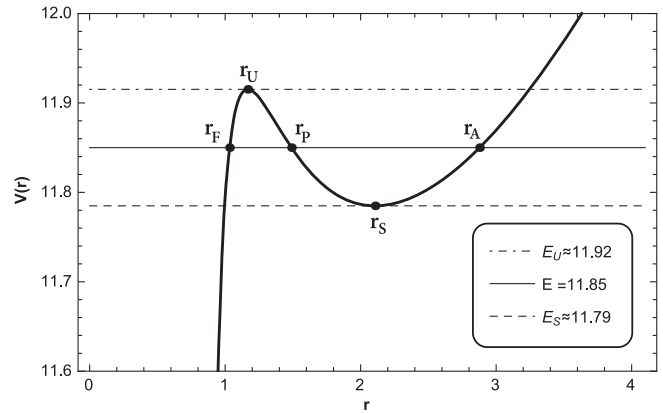


FIG. 5. The behavior of $V(r)$ as a function of r , for $L = 12$, $M = a = b = \lambda = 1$, $J = 1.2$, $\xi = 1.1$, $r_F \approx 1.03$, $r_U \approx 1.17$, $r_P \approx 1.49$, $r_S \approx 2.11$, $r_A \approx 2.88$, $E = 11.85$, $E_S = 11.79$, $E_U = 11.92$, and $\Lambda = -1$.

$$r_A = \left(\frac{\alpha}{3} + 2\sqrt{\frac{A}{3}} \cos \left[\frac{1}{3} \cos^{-1} \left[\frac{3B}{2} \sqrt{\frac{3}{A^3}} \right] \right] \right)^{1/2}, \quad (37)$$

$$r_P = \left(\frac{\alpha}{3} + 2\sqrt{\frac{A}{3}} \cos \left[\frac{1}{3} \cos^{-1} \left[\frac{3B}{2} \sqrt{\frac{3}{A^3}} + \frac{4\pi}{3} \right] \right] \right)^{1/2}, \quad (38)$$

and

$$r_F = \left(\frac{\alpha}{3} + 2\sqrt{\frac{A}{3}} \cos \left[\frac{1}{3} \cos^{-1} \left[\frac{3B}{2} \sqrt{\frac{3}{A^3}} + \frac{2\pi}{3} \right] \right] \right)^{1/2}, \quad (39)$$

where $A = \frac{\alpha^2}{3} + \beta$ and $B = \frac{2\alpha^3}{27} + \frac{\alpha\beta}{3} + \gamma$. Now, we will determine the angular coordinate of the trajectory for a particle that starts at $r = r_A$, and it is given by the solution of the integral

$$\phi(r) = - \int_{r_A}^r \frac{r^2}{(-\bar{\Lambda})(r^2 - r_+^2)(r^2 - r_-^2)} \times \left[-L\bar{\Lambda}r^2 + \left(\frac{EJ}{2} - ML \right) - L \frac{J^2 - \bar{J}^2}{4r^2} \right] \frac{dr}{\sqrt{P(r)}}, \quad (40)$$

where we have used Eqs. (22) and (24), and whose solution is

$$\phi(r) = k_0 \Psi_0(r) + K_0 [k_+ \Psi_+(r) - k_- \Psi_-(r)], \quad (41)$$

where

$$k_0 = \frac{r_A L (J^2 - \bar{J}^2)}{8(-\bar{\Lambda})^{3/2} \sqrt{\bar{\gamma}} r_+^2 r_-^2},$$

$$\Psi_0(r) = \wp^{-1}[U(r_A)] - \wp^{-1}[U(r)], \quad (42)$$

$$k_{\pm} = \frac{EJ/2 - LM}{r_{\pm}^2} - \bar{\Lambda}L - \frac{L(J^2 - \bar{J}^2)}{4r_{\pm}^4}. \quad (43)$$

This solution is plotted in Fig. 6 for direct orbits, where we can observe the trajectory of the first and second kinds. Note that the coordinate (ϕ) diverges at the event horizon. Also, the solution (41) allows us to determine the precession angle, by considering that it is given by $\Theta = 2\phi_P - 2\pi$, where ϕ_P is the angle from the apoastron to the periastron. Thus, we obtain

$$\Theta = 2k_0\Psi_0(r_P) + 2K_0[k_+\Psi_+(r_P) - k_-\Psi_-(r_P)] - 2\pi. \quad (44)$$

This is an exact solution for the angle of precession, and it depends on the spacetime parameters M , J , and \bar{J} and the particle motion constants E and L .

In Fig. 7, we plot the behavior of the retrograde orbits, where clearly they correspond to second kind trajectories. Here, we can observe the effect of the dragging of inertial frames. The test particle starts at $r = r_A$, then at $r = R$ the

angular velocity is null, and $\phi(r)$ is maximum; after that the angle $\phi(r)$ decreases and tends to $-\infty$, when $r \rightarrow r_+$.

Now, in order to determine the proper and coordinate period of rotation of the trajectories, we present the solution for both times. The proper time (τ) is given by the solution of the integral

$$\tau(r) = - \int_{r_A}^r \frac{r^2 dr}{\sqrt{P(r)}}, \quad (45)$$

where we have used Eq. (24) and we have considered as initial conditions that the particles are at $r = r_A$ when $\phi = t = \tau = 0$. Thus, we obtain

$$\tau(r) = \frac{r_A^3}{8\sqrt{(-\Lambda)\gamma}} (\Psi[U(r), \Omega] - \Psi[U(r_A), \Omega]), \quad (46)$$

where

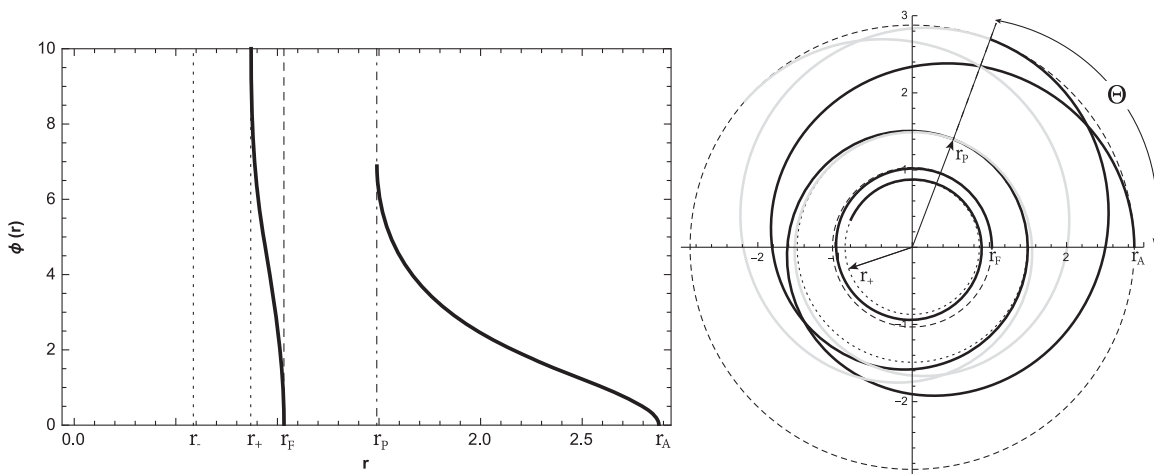


FIG. 6. Direct orbits. The behavior of $\phi(r)$ (left) and $r(\phi)$ (right) for bounded orbits of the first and second kind with $E = 11.85$, $L = 12$, $M = a = b = \lambda = 1$, $\Lambda = -1$, $J = 1.2$, and $\xi = 1.1$.

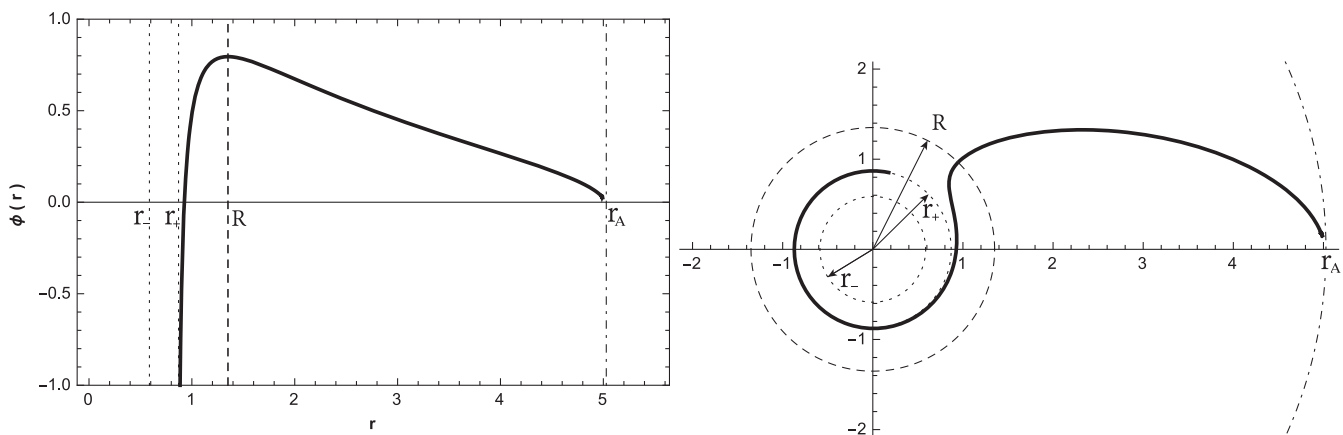


FIG. 7. Retrograde orbits. The behavior of $\phi(r)$ (left) and $r(\phi)$ (right) for bounded orbits of the second kind with $E = 11.85$, $L = 12$, $M = a = b = \lambda = 1$, $\Lambda = -1$, $J = -1.2$, $R = 1.35$, and $\xi = 1.1$.

$$\Psi(U, \Omega) = \frac{1}{\wp'(\Omega)} \left[2\zeta(\Omega)\wp^{-1}(U) + \ln \left| \frac{\sigma[\wp^{-1}(U) - \Omega]}{\sigma[\wp^{-1}(U) + \Omega]} \right| \right], \quad (47)$$

and

$$U(r) = \frac{r_A^2}{4r^2} + \frac{\beta r_A^2}{12\gamma}, \quad U(r_A) = \frac{1}{4} + \frac{\beta r_A^2}{12\gamma}, \quad (48)$$

$$\Omega = \wp^{-1} \left[\frac{\beta r_A^2}{12\gamma} \right], \quad (49)$$

$$g_2 = \frac{r_A^4}{4} \left[\frac{\beta^2}{3\gamma^2} - \frac{\alpha}{\gamma} \right], \quad g_3 = \frac{r_A^6}{16} \left[\frac{\alpha\beta}{3\gamma^2} - \frac{2\beta^3}{27\gamma^3} + \frac{1}{\gamma} \right]. \quad (50)$$

In Fig. 8, we show the behavior of the proper time as a function of r for direct orbits (Fig. 8, left). We can observe, for the trajectory of the first and second kind, the particle arrives in a finite proper time to r_p and to reach the singularity, respectively. Also, the period of a revolution according to the proper time is $T_\tau = 2\tau(r_p)$. Concerning the retrograde orbits (Fig. 8, right), for the trajectory of the second kind, the particle arrives in a finite proper time to the singularity.

On the other hand, by considering Eqs. (23) and (24), and as initial condition that the particles are at $r = r_A$ when $\phi = t = \tau = 0$, the coordinate time (t) is

$$t(r) = - \int_{r_A}^r \frac{r^2 [Er^2 - JL/2]}{(-\Lambda)(r^2 - r_+^2)(r^2 - r_-^2) \sqrt{P(r)}} dr, \quad (51)$$

whose solution is

$$t(r) = K_0 \left[\left(E - \frac{JL}{2r_+^2} \right) \Psi_+(r) - \left(E - \frac{JL}{2r_-^2} \right) \Psi_-(r) \right], \quad (52)$$

where $K_0 = \frac{r_A^3}{8(-\Lambda)^{3/2} \sqrt{\gamma(r_+^2 - r_-^2)}}$, and

$$\Psi_\pm(r) = \Psi[U(r_A), \Omega_\pm] - \Psi[U(r), \Omega_\pm],$$

$$\Omega_\pm(r) = \wp^{-1} \left[\frac{r_A^2}{4r_\pm^2} + \frac{\beta r_A^2}{12\gamma} \right]. \quad (53)$$

Also, in Fig. 8, we show the behavior of the coordinate time as a function of r . For direct orbits, we can observe, for the trajectory of the first and second kind, the particle arrives in a finite and infinity coordinate time to r_p and r_+ , respectively. Also, the period of a revolution according to the coordinate time is $T_t = 2t(r_p)$. Concerning the retrograde orbits (Fig. 8, right), for the trajectory of the second kind, the particle arrives in an infinite coordinate time to r_+ . Also, we can observe that the zero located at R does not affect the proper and coordinate times.

B. Circular orbits

The effective potential $V(r)$ has to exhibit extrema for fixed values of radial coordinate $r = r_{c.o.}$, when

$$\left. \frac{dV(r)}{dr} \right|_{r_{c.o.}} = 0. \quad (54)$$

Now, for simplicity, we write the effective potential as

$$V(r) = \frac{JL}{2r^2} + \sqrt{\mathcal{F}(r) + L^2 \frac{\mathcal{F}(r)}{r^2}}. \quad (55)$$

Therefore, using Eq. (55) into Eq. (54) yields

$$\left[r^3 \mathcal{F}'(r) + L^2 [r \mathcal{F}'(r) - 2\mathcal{F}(r)] - 2JL \sqrt{\mathcal{F}(r) + L^2 \frac{\mathcal{F}(r)}{r^2}} \right] \Big|_{r_{c.o.}} = 0. \quad (56)$$

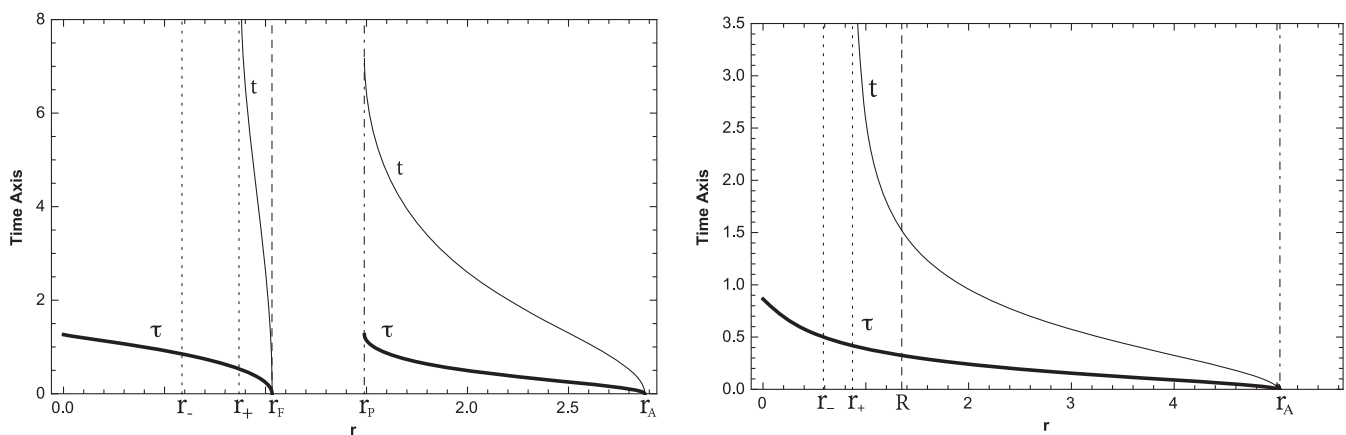


FIG. 8. The behavior of the coordinate time (t) and the proper time (τ) along a bounded timelike geodesic described by a test particle, starting at r_A , and $r_F = 1.03$ with $r_p = 1.49$, $R = 1.35$, $L = 12$, $M = a = b = \lambda = 1$, $\Lambda = -1$, $E = 11.85$, $\xi = 1.1$, $r_+ \approx 0.87$, and $r_- \approx 0.59$. Left: direct orbits with $J = 1.2$ and $r_A = 2.88$. Right: retrograde orbits with $J = -1.2$ and $r_A = 5.03$.

Notice that this equation leads to a polynomial of twelfth grade given by

$$r_{c.o.}^{12} + \frac{\bar{J}^2 - 4L^2M}{2\bar{\Lambda}} r_{c.o.}^8 + \frac{L^2(J^2 + \bar{J}^2)}{\bar{\Lambda}} r_{c.o.}^6 + \frac{16J^2L^2(\bar{\Lambda}L^2 + M) + \bar{J}^2(\bar{J}^2 - 8L^2M) + 16L^4M^2}{16\bar{\Lambda}^2} r_{c.o.}^4 + \frac{L^2(J^2 - \bar{J}^2)(4L^2M - \bar{J}^2)}{4\bar{\Lambda}^2} r_{c.o.}^2 - \frac{\bar{J}^2L^4(J^2 - \bar{J}^2)}{4\bar{\Lambda}^2} = 0, \quad (57)$$

so it is possible to find the roots numerically. On the other hand, condition (56) allows us to obtain the angular momentum for the stable $L_{c.o.} = L_S$ at $r_{c.o.} = r_S$ and for the unstable circular orbits $L_{c.o.} = L_U$ at $r_{c.o.} = r_U$, which yields

$$AL_{c.o.}^4 - BL_{c.o.}^2 + C = 0, \quad (58)$$

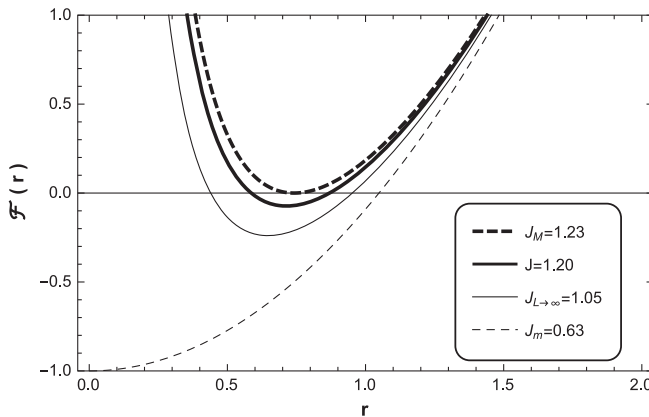
where

$$A = \left[4(M^2 + \bar{\Lambda}J^2) + (J^2 - \bar{J}^2) \left(\frac{4M}{r^2} - \frac{\bar{J}^2}{r^4} \right) \right] \Big|_{r_{c.o.}},$$

$$B = \left[\frac{\bar{J}^2}{r^2} (J^2 - \bar{J}^2) - 2M(2J^2 - \bar{J}^2) - 4\bar{\Lambda}r^2(J^2 + \bar{J}^2 - 2Mr^2) \right] \Big|_{r_{c.o.}},$$

$$C = \left[4\bar{\Lambda}^2r^8 + 2\bar{\Lambda}\bar{J}^2r^4 + \frac{\bar{J}^2}{4} \right] \Big|_{r_{c.o.}}. \quad (59)$$

Thus, the real solution of the quartic equation for $L_{c.o.}$ is



$$L_{c.o.}^2 = \left[\frac{B - \sqrt{B^2 - 4AC}}{2A} \right] \Big|_{r_{c.o.}}, \quad (60)$$

and the energy is given by $E_{c.o.} = JL_{c.o.}/2r_{c.o.}^2 + \sqrt{\mathcal{F}(r_{c.o.}) + L_{c.o.}^2\mathcal{F}(r_{c.o.})/r_{c.o.}^2}$.

Now, in Fig. 9, we show the behavior of the lapse function and the effective potential for different values of J . We can observe that J cannot take big values due to the spacetime becomes in a naked singularity, and for a very small value of J , the black hole presents only one event horizon, because the \bar{J}^2 became negative. So, only in spacetimes with sufficiently big $|J|$ do the circular corotating orbits in the domain $r > r_+$ exist.

Also, the behavior of the effective potential for different values of angular momentum L is shown in Fig. 10. We can observe that, for $L > L_{LSCO}$, when the angular momentum increases the radius of the stable circular orbit increases, and the radius of the unstable circular orbit (r_U) decreases. Also, when $L \rightarrow \infty$ the $r_U \rightarrow R_U$ is given by

$$R_U = \left[\frac{-M(J^2 - \bar{J}^2) - |J|\sqrt{(J^2 - \bar{J}^2)(M^2 + \bar{\Lambda}\bar{J}^2)}}{2(M^2 + \bar{\Lambda}\bar{J}^2)} \right]^{1/2}, \quad (61)$$

which corresponds to the minimum radius for this orbit. Note that the above equation diverges at $J = J_{L \rightarrow \infty} = \sqrt{-M^2/\bar{\Lambda}}$. Also, for $J^2 < -M^2/\bar{\Lambda}$, R_U became imaginary. On the other hand, the radius of the last stable circular orbit must satisfied $V'|_{r_{LSCO}, L_{LSCO}} = 0$ and $V''|_{r_{LSCO}, L_{LSCO}} = 0$, and it is given by

$$r_{LSCO} = \left[\frac{L_{LSCO}^2(J^2 - \bar{J}^2)}{4(-\bar{\Lambda})} \right]^{1/6}. \quad (62)$$

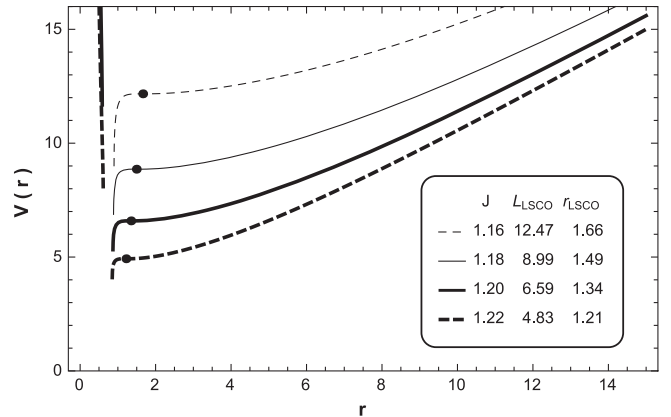


FIG. 9. The behavior of the lapse function (left) and the behavior of $V(r)$ (right) as a function of r , for different values of the angular momentum of the black hole J , with $M = a = b = \lambda = 1$, $\xi = 1.1$, and $\Lambda = -1$. For $J = J_m = 2a\sqrt{\xi - 1}$, the black hole has one horizon at $r = r_+ = 1.05$; in the range $J_m < J < J_M$, the black hole has two horizons at $r = r_- = 0.40$ and $r = r_+ = 0.97$; and for $J = J_M = \sqrt{\frac{4a^2\bar{\Lambda}(\xi - 1) - M^2\xi}{\bar{\Lambda}}}$, the black hole is extremal at $r = r_e = 0.74$. $J = J_{L \rightarrow \infty} = \sqrt{-M^2/\bar{\Lambda}}$ corresponds to the value of J for which the minimum radius of the stable circular orbit diverges, see Eq. (61).

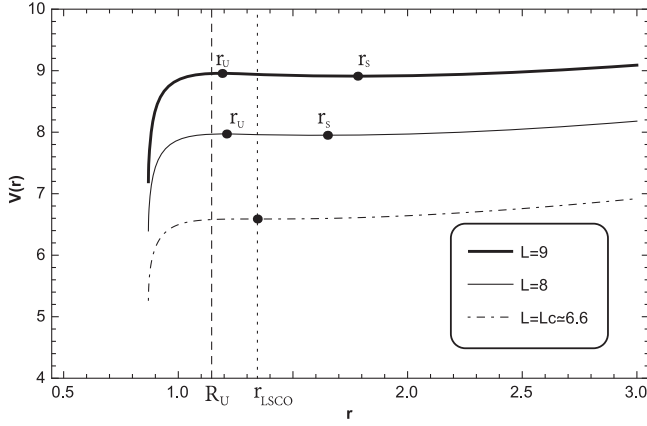


FIG. 10. The behavior of $V(r)$ as a function of r , for different values of the angular momentum of the particle L , with $M = a = b = \lambda = 1$, $\xi = 1.1$, $r_+ \approx 0.87$, $J = 1.2$, $\Lambda = -1$, $R_U = 1.15$, and $r_{\text{LSCO}} = 1.34$. For $L = 8$, $r_U = 1.21$ and $r_S = 1.65$. For $L = 9$, $r_U = 1.19$ and $r_S = 1.78$. Here, $L_c = L_{\text{LSCO}}$.

Therefore, in the range $J_{L \rightarrow \infty} < J < J_M$ the black hole has two horizons and the effective potential allows circular and planetary orbits for $L > L_{\text{LSCO}}$.

Also, it is possible to determine the periods of revolution of the circular orbits, both stable and unstable, with respect to the proper time τ , $T_\tau = 2\pi/\dot{\phi}(r_{\text{c.o.}})$, and coordinate time t , $T_t = T_\tau \dot{t}(r_{\text{c.o.}})$. Thereby, the period of a revolution according to the proper time is

$$T_\tau = \frac{4\pi(-\bar{\Lambda})r_{\text{c.o.}}(r_{\text{c.o.}}^2 - r_+^2)(r_{\text{c.o.}}^2 - r_-^2)}{J\sqrt{(r_{\text{c.o.}}^2 + L_{\text{c.o.}}^2)\mathcal{F}(r_{\text{c.o.}}) + 2L_{\text{c.o.}}r_{\text{c.o.}}\mathcal{F}(r_{\text{c.o.}})}}, \quad (63)$$

and the period according to the coordinate time is

$$T_t = \frac{4\pi r_{\text{c.o.}}^2 \sqrt{(r_{\text{c.o.}}^2 + L_{\text{c.o.}}^2)\mathcal{F}(r_{\text{c.o.}})}}{J\sqrt{(r_{\text{c.o.}}^2 + L_{\text{c.o.}}^2)\mathcal{F}(r_{\text{c.o.}}) + 2L_{\text{c.o.}}r_{\text{c.o.}}\mathcal{F}(r_{\text{c.o.}})}}. \quad (64)$$

On the other hand, Taylor expanding the effective potential around $r = r_S$, one can write $V(r) = V(r_S) + V'(r_S)(r - r_S) + \frac{1}{2}V''(r_S)(r - r_S)^2 + \dots$, where $'$ means derivative with respect to the radial coordinate. Obviously, in these orbits $V'(r_S) = 0$; so, by defining the *smaller* coordinate $x = r - r_S$, together with the epicycle frequency $\kappa^2 = V''(r_S)$ [21], we can rewrite the above equation as $V(x) \approx E_S + \kappa^2 x^2/2$, where E_S is the energy of the particle in the stable circular orbit. Also, it is easy to see that test particles satisfy the harmonic equation of motion $\ddot{x} = -\kappa^2 x$. Therefore, the epicycle frequency is given by

$$\kappa^2 = \frac{JL_{\text{c.o.}}}{r^4} \left[3 + \frac{r^4 \mathcal{F}'' + r^2 L_{\text{c.o.}}^2 \mathcal{F}'' - 4r \mathcal{F}' L_{\text{c.o.}}^2 + 6L_{\text{c.o.}}^2 \mathcal{F}}{r^3 \mathcal{F}' + r \mathcal{F}' L_{\text{c.o.}}^2 - 2L_{\text{c.o.}}^2 \mathcal{F}} - \frac{r^3 \mathcal{F}' + r \mathcal{F}' L_{\text{c.o.}}^2 - 2L_{\text{c.o.}}^2 \mathcal{F}}{2(r^2 \mathcal{F} + L_{\text{c.o.}}^2 \mathcal{F})} \right] \Big|_{r_S}. \quad (65)$$

In the case of nonrotating black holes, the polynomial (57) has an analytical solution and at $r = r_{\text{ext}}$ can be written as

$$r_{\text{ext}}^6 + \frac{1}{\bar{\Lambda}} \left(\frac{\bar{J}^2}{4} - M\bar{L}^2 \right) r_{\text{ext}}^2 + \frac{\bar{J}^2 \bar{L}^2}{2\bar{\Lambda}} = 0, \quad (66)$$

where the quadratic term is null for $L = L_1 = \frac{\bar{J}}{2\sqrt{M}}$. The root of this polynomial is

$$r_{\text{ext}} = \left(\sqrt{\frac{\chi_2}{3}} \cosh \left[\frac{1}{3} \cosh^{-1} \left(3\chi_3 \sqrt{\frac{3}{\chi_2^3}} \right) \right] \right)^{1/2}, \quad (67)$$

for $0 < L < L_1$,

$$r_{\text{ext}} = \left(\frac{\bar{J}^2 L_1^2}{-2\bar{\Lambda}} \right)^{1/6} = \left(\frac{\bar{J}^4}{-8M\bar{\Lambda}} \right)^{1/6}, \quad (68)$$

for $L = L_1$, and

$$r_{\text{ext}} = \left(\sqrt{\frac{-\chi_2}{3}} \sinh \left[\frac{1}{3} \sinh^{-1} \left(3\chi_3 \sqrt{\frac{3}{-\chi_2^3}} \right) \right] \right)^{1/2}, \quad (69)$$

for $L > L_1$, where

$$\chi_2 = -\frac{4}{\bar{\Lambda}} \left(\frac{\bar{J}^2}{4} - M\bar{L}^2 \right), \quad \chi_3 = -\frac{2\bar{J}^2 \bar{L}^2}{\bar{\Lambda}}. \quad (70)$$

In Fig. 11 we show the behavior of the effective potential for nonrotating black holes for large and small values of L , and in Fig. 12, we show that the lapse function at $r = r_{\text{ext}}$ is negative for different values of L . Therefore, for $J = 0$, we have shown that there are no circular orbits in the domain $r > r_+$.

On the other hand, in Fig. 13, we show that there is no circular orbit in the relevant domain $r > r_+$, for black holes with one horizon (Fig. 13, left) and for black holes with an inner and outer horizon (Fig. 13, right). Moreover, in this domain, the behavior for a nonrotating black hole is similar to the behavior for small values of $|J|$.

C. Critical trajectories

There are two critical orbits that approach the unstable circular orbit asymptotically. In the first kind, the particle arises from $r = r_A$, and in the second kind, the particle starts from a finite distance $r = r_i$: bigger than the horizon radius, but smaller than the unstable radius, see Fig. 14.

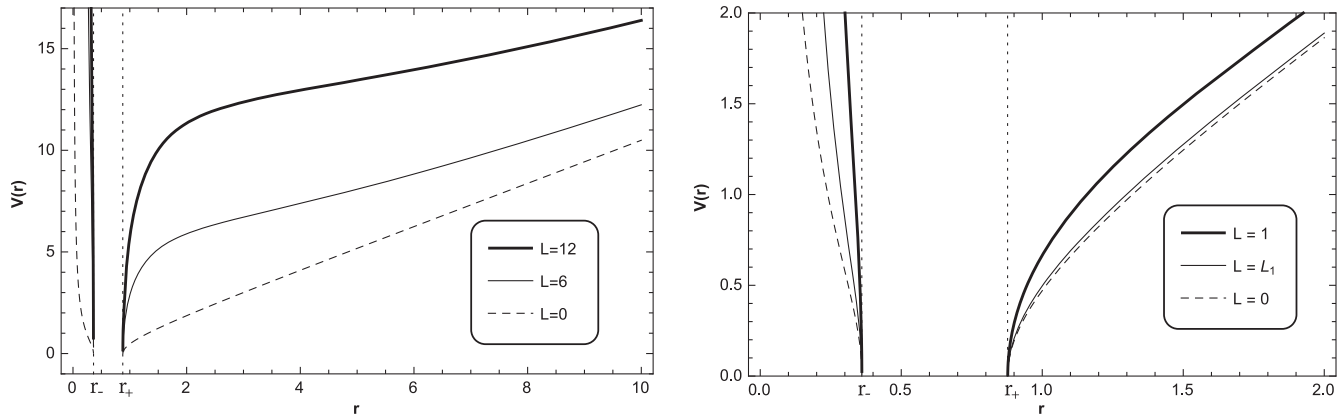


FIG. 11. The behavior of $V(r)$ as a function of r , for different values of the angular momentum of the particle L , with $M = a = b = \lambda = 1$, $J = 0$, $\xi = 0.9$, and $\Lambda = -1$. Here $r_+ = 0.878$, $r_- = 0.360$, and $L_1 = 0.333$.

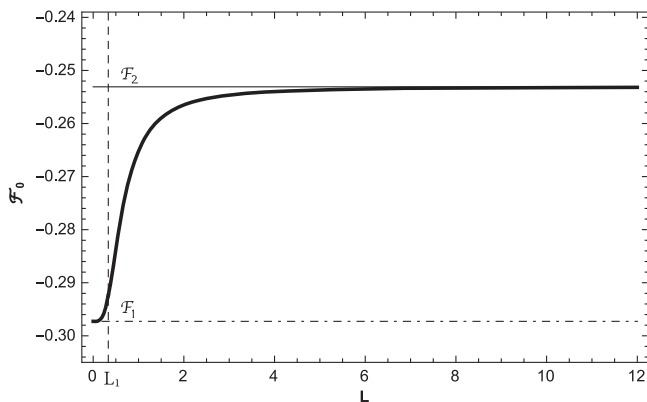


FIG. 12. The behavior of $\mathcal{F}_0(L)$ as a function of L , with $M = a = b = \lambda = 1$, $J = 0$, $\xi = 0.9$, $L_1 = 0.333$, and $\Lambda = -1$. The metric function at $r = r_{\text{ext}}$ tends to $\mathcal{F}_2 = -0.253$ when $L \rightarrow \infty$ and it tends to $\mathcal{F}_1 = -0.297$ when $L \rightarrow 0$. Here, the function $\mathcal{F}_0(L) = \mathcal{F}[r_{\text{ext}}(L)]$, where $\mathcal{F}_1 = \mathcal{F}_0(L \rightarrow 0) = -M + \bar{J} \sqrt{-\Lambda}$, and $\mathcal{F}_2 = \mathcal{F}_0(L \rightarrow \infty) = -\frac{M}{2} + \frac{J^2(-\Lambda)}{2M}$.

By considering $\phi = t = \tau = 0$ and Eq. (24), the proper time for the critical orbit of the first kind is

$$\tau(r) = -\frac{1}{(-\Lambda)^{1/2}} \int_{r_A}^r \frac{r^2 dr}{(r^2 - r_U^2) \sqrt{r_A^2 - r^2}}, \quad (71)$$

whose solution is given by

$$\tau(r) = \frac{1}{\sqrt{-\Lambda}} \left[\psi(r) + \frac{r_U}{\sqrt{r_A^2 - r_U^2}} \psi_U(r) \right], \quad (72)$$

where

$$\psi[r] = \tan^{-1} \sqrt{\frac{r_A^2}{r^2} - 1}, \quad (73)$$

and

$$\psi_U[r] = \tanh^{-1} \left[\frac{r_U}{r} \sqrt{\frac{r_A^2 - r^2}{r_A^2 - r_U^2}} \right]. \quad (74)$$

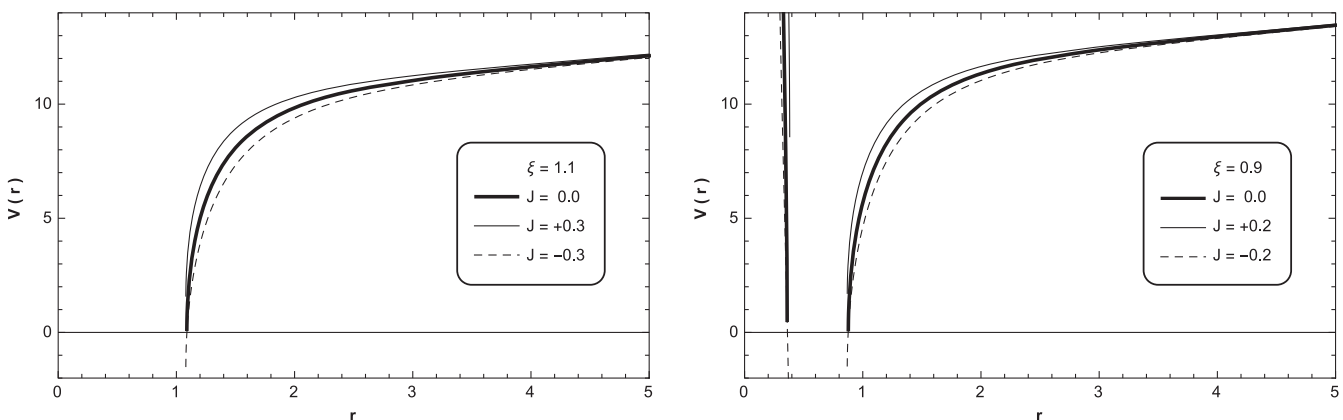


FIG. 13. The behavior of the effective potential $V(r)$ as a function of r , for different values of the angular momentum of the black hole J , with $M = a = b = \lambda = 1$, $\Lambda = -1$, and $L = 12$. Left: $\xi = 1.1$. Right: $\xi = 0.9$.

Now, for the critical trajectories of the second kind, the proper time is

$$\tau(r) = \frac{1}{\sqrt{(-\bar{\Lambda})}} \left[\psi(r) - \psi(r_i) + \frac{r_U [\psi_U(r) - \psi_U(r_i)]}{\sqrt{r_A^2 - r_U^2}} \right]. \quad (75)$$

On the other hand, by considering $\phi = t = \tau = 0$, Eqs. (23) and (24), the coordinate time for the critical trajectory of the first kind is

$$t(r) = - \int_{r_A}^r \frac{r^2 [Er^2 - JL/2] dr}{(-\bar{\Lambda})^{3/2} (r^2 - r_+^2)(r^2 - r_-^2)(r^2 - r_U^2) \sqrt{r_A^2 - r^2}}, \quad (76)$$

whose solution is

$$t(r) = \frac{1}{(-\bar{\Lambda})^{3/2}} \sum_{j=1}^3 \tilde{k}_j \psi_j(r), \quad (77)$$

where

$$\psi_1(r) = \frac{r_U}{\sqrt{r_A^2 - r_U^2}} \tanh^{-1} \left[\frac{r_U}{r} \sqrt{\frac{r_A^2 - r^2}{r_A^2 - r_U^2}} \right], \quad (78)$$

$$\psi_2(r) = \frac{r_+}{\sqrt{r_A^2 - r_+^2}} \tanh^{-1} \left[\frac{r_+}{r} \sqrt{\frac{r_A^2 - r^2}{r_A^2 - r_+^2}} \right], \quad (79)$$

$$\psi_3(r) = \frac{r_-}{\sqrt{r_A^2 - r_-^2}} \tanh^{-1} \left[\frac{r_-}{r} \sqrt{\frac{r_A^2 - r^2}{r_A^2 - r_-^2}} \right], \quad (80)$$

and

$$\begin{aligned} \tilde{k}_1 &= \frac{Er_U^2 - JL/2}{(r_U^2 - r_+^2)(r_U^2 - r_-^2)}, \\ \tilde{k}_2 &= - \frac{Er_+^2 - JL/2}{(r_U^2 - r_+^2)(r_+^2 - r_-^2)}, \\ \tilde{k}_3 &= \frac{Er_-^2 - JL/2}{(r_U^2 - r_-^2)(r_+^2 - r_-^2)}. \end{aligned} \quad (81)$$

For the critical trajectories of the second kind, the coordinate time is

$$t(r) = \frac{1}{(-\bar{\Lambda})^{3/2}} \sum_{j=1}^3 \tilde{k}_j [\psi_j(r) - \psi_j(r_i)]. \quad (82)$$

In Fig. 14, we plot the behavior of the proper and coordinate time as a function of r . We observe that, for both times, the particle takes an infinity time to arrive to the unstable circular orbit. Finally, by using Eqs. (22), and (24),

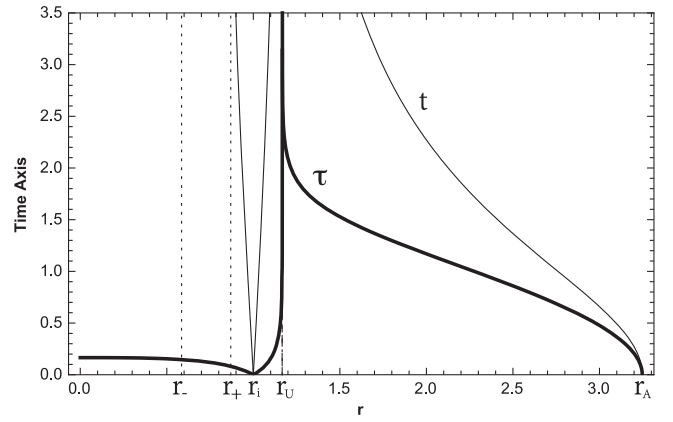


FIG. 14. The behavior of the proper (τ) (thick line) and coordinate (t) (thin line) time as a function of r for critical trajectories of the first and second kind with $M = a = b = \lambda = 1$, $\Lambda = -1$, $J = 1.2$, $\xi = 1.1$, $r_- \approx 0.59$, $r_+ \approx 0.87$, $r_i = 1.00$, $r_U \approx 1.17$, $r_A \approx 3.25$, and $E_U \approx 11.92$.

the angular coordinate ϕ for the trajectories of the first kind is

$$\phi_C(r) = \frac{1}{(-\bar{\Lambda})^{3/2}} \sum_{i=1}^3 \eta_i \psi_i(r), \quad (83)$$

where

$$\begin{aligned} \eta_1 &= \frac{1}{(r_U^2 - r_+^2)(r_U^2 - r_-^2)} \\ &\times \left(\frac{E_U J}{2} - LM + (-\bar{\Lambda}) L r_U^2 - \frac{L(J^2 - \bar{J}^2)}{4r_U^2} \right), \end{aligned} \quad (84)$$

$$\begin{aligned} \eta_2 &= \frac{-1}{(r_U^2 - r_+^2)(r_+^2 - r_-^2)} \\ &\times \left(\frac{E_U J}{2} - LM + (-\bar{\Lambda}) L r_+^2 - \frac{L(J^2 - \bar{J}^2)}{4r_+^2} \right), \end{aligned} \quad (85)$$

$$\begin{aligned} \eta_3 &= \frac{1}{(r_U^2 - r_-^2)(r_+^2 - r_-^2)} \\ &\times \left(\frac{E_U J}{2} - LM + (-\bar{\Lambda}) L r_-^2 - \frac{L(J^2 - \bar{J}^2)}{4r_-^2} \right). \end{aligned} \quad (86)$$

While that for critical trajectories of the second kind is

$$\phi_C(r) = \frac{1}{(-\bar{\Lambda})^{3/2}} \sum_{j=1}^3 \eta_j [\psi_j(r) - \psi_j(r_i)]. \quad (87)$$

In Fig. 15, we show the behavior of the angular coordinate as a function of r . We can observe that, for both trajectories of the first and second kind, the angular coordinate diverges at the unstable circular radius.

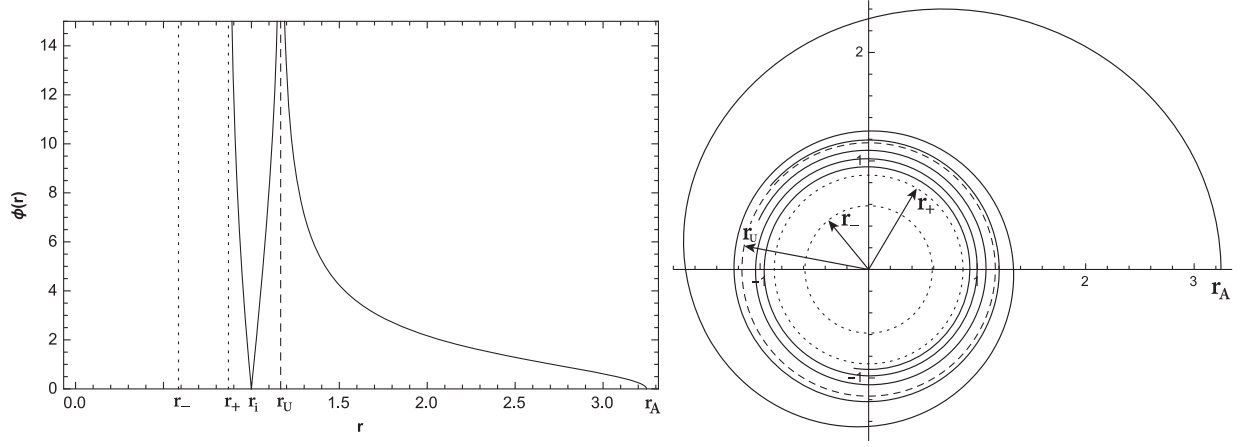


FIG. 15. Critical trajectory of the first and second kind, for particles with $L = 12$, $M = a = b = \lambda = 1$, $\Lambda = -1$, $J = 1.2$, $\xi = 1.1$, $E_U = 11.92$, $r_- \approx 0.59$, $r_+ \approx 0.87$, and $r_i = 1.0$. For orbit of the first kind (thin line), the test particle arrived from $r_A = 3.25$, where $r_U \approx 1.17$ corresponds to the radius of the unstable circular orbit (dashed circle).

D. Motion with $L=0$

In this case, the particles are destined to fall toward the event horizon, see Fig. 5. The effective potential Eq. (25) is $V(r) = (-M + \frac{\bar{J}^2}{4r^2} - \bar{\Lambda}r^2)^{1/2}$, and Eqs. (22)–(24) yield

$$\dot{\phi} = -\frac{EJ}{2\bar{\Lambda}(r^2 - r_+^2)(r^2 - r_-^2)}, \quad (88)$$

$$\dot{t} = -\frac{Er^2}{\bar{\Lambda}(r^2 - r_+^2)(r^2 - r_-^2)}, \quad (89)$$

$$\pm \dot{r} = \sqrt{E^2 + M - \frac{\bar{J}^2}{2r^2} + \bar{\Lambda}r^2}, \quad (90)$$

where the $(-)$ sign for \dot{r} corresponds to particles falling into the event horizon, and the $(+)$ sign corresponds to particles that have a return point $r_0 > r_+$, for $E > E_+$, given by

$$r_0 = \sqrt{\frac{M + E^2}{-\bar{\Lambda}}} \sin \left[\frac{1}{2} \sin^{-1} \left(\frac{\bar{J} \sqrt{-\bar{\Lambda}}}{M + E^2} \right) + \frac{\pi}{2} \right], \quad (91)$$

and a return point at $d_0 < r_-$, given by

$$d_0 = \sqrt{\frac{M + E^2}{-\bar{\Lambda}}} \sin \left[\frac{1}{2} \sin^{-1} \left(\frac{\bar{J} \sqrt{-\bar{\Lambda}}}{M + E^2} \right) \right]. \quad (92)$$

Now, choosing as initial conditions that the particle starts at $r = r_0$ and $\phi = t = \tau = 0$, the solution of Eq. (90) is

$$\tau(r) = \frac{1}{2\sqrt{-\bar{\Lambda}}} \left(\sin^{-1} \left[\frac{M + 2\bar{\Lambda}r^2 + E^2}{\sqrt{\bar{J}^2\bar{\Lambda} + (M + E^2)^2}} \right] - \sin^{-1} \left[\frac{M + 2\bar{\Lambda}r_0^2 + E^2}{\sqrt{\bar{J}^2\bar{\Lambda} + (M + E^2)^2}} \right] \right). \quad (93)$$

Also, a straightforward integration of Eqs. (89) and (90) leads to

$$t(r) = \frac{E}{2(-\bar{\Lambda})^{3/2}} \left[\frac{r_+^2}{\sqrt{p(r_+)}} \ln \left| \frac{r_0^2 - r_+^2}{r^2 - r_+^2} \cdot \frac{F_+(r)}{F_+(r_0)} \right| - \frac{r_-^2}{\sqrt{p(r_-)}} \ln \left| \frac{r_0^2 - r_-^2}{r^2 - r_-^2} \cdot \frac{F_-(r)}{F_-(r_0)} \right| \right], \quad (94)$$

where

$$F_{\pm}(r) = 2p(r_{\pm}) + \left(\frac{E^2 + M}{-\bar{\Lambda}} - 2r_{\pm}^2 \right) (r^2 - r_{\pm}^2) + 2\sqrt{p(r_{\pm})}\sqrt{P_{\pm}(r)}, \quad (95)$$

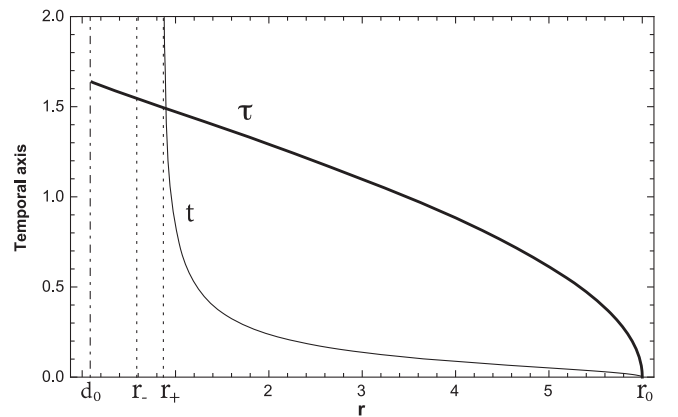


FIG. 16. The behavior of the coordinate time (t) and the proper time (τ) along an unbounded timelike radial geodesic described by a test particle, starting at $r_0 = 6$ and falling toward the singularity, for $L = 0$, $M = a = b = \lambda = 1$, $\Lambda = -1$, $E = 5.63$, $J = 1.2$, $\xi = 1.1$, $r_+ \approx 0.87$, $d_0 = 0.085$, and $r_- \approx 0.59$.

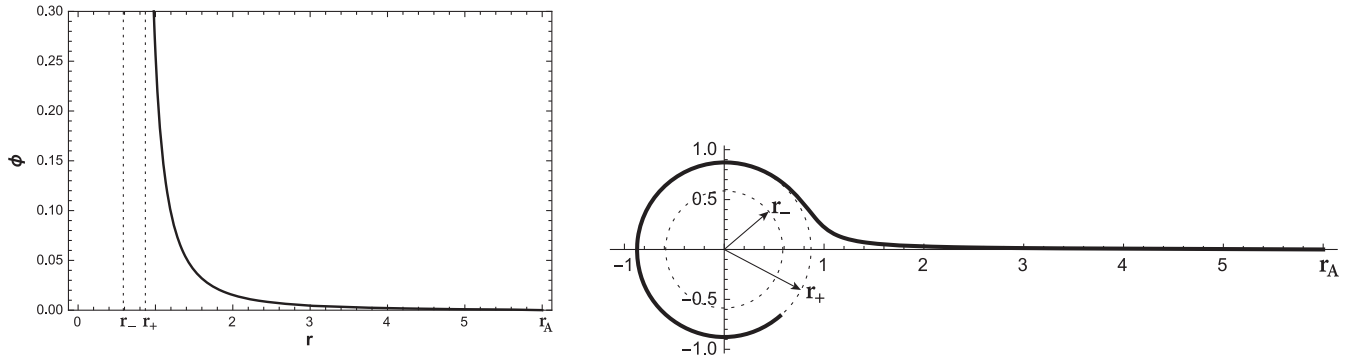


FIG. 17. The behavior of the coordinate $\phi(r)$, starting at $r_0 = 6$ and falling toward the singularity with $L = 0$, $M = a = b = \lambda = 1$, $\Lambda = -1$, $J = 1.2$, $\xi = 1.1$, $r_- \approx 0.59$, and $r_+ = 0.87$. In the polar plot, the trajectory approaching the horizon will spiral around the black hole an infinite number of times.

$$p(r) = -r^4 + \frac{E^2 + M}{-\Lambda} r^2 - \frac{\bar{J}^2}{4(-\Lambda)}, \quad (96)$$

$$P_{\pm}(r) = p(r_{\pm}) + \left(\frac{E^2 + M}{-\Lambda} - 2r_{\pm}^2 \right) (r^2 - r_{\pm}^2) - (r^2 - r_{\pm}^2)^2. \quad (97)$$

In Fig. 16, we show the behavior of the proper and coordinate time as a function of r ; we can observe that the particle arrives to the event horizon in a finite proper time, then the particle does not reach the singularity, due to the existence of a return point d_0 inside r_- , see Fig. 4. Concerning the coordinate time, the particle arrives in an infinite coordinate time to the singularity. Finally, the solution for the angular coordinate ϕ is

$$\phi(r) = \frac{EJ}{4(-\Lambda)^{3/2}} \left[\frac{1}{\sqrt{p(r_+)}} \ln \left| \frac{r_0^2 - r_+^2}{r^2 - r_+^2} \cdot \frac{F_+(r)}{F_+(r_0)} \right| - \frac{1}{\sqrt{p(r_-)}} \ln \left| \frac{r_0^2 - r_-^2}{r^2 - r_-^2} \cdot \frac{F_-(r)}{F_-(r_0)} \right| \right], \quad (98)$$

where we have used Eqs. (88) and (90). In Fig. 17, we plot the behavior of the angular coordinate, where we observe that the angular coordinate becomes infinity at the event horizon.

V. REMARKS AND CONCLUSIONS

In this work, we studied the motion of particles in the background of a rotating three-dimensional Hořava AdS black hole described by a Lorentz-violating version of the BTZ black hole, and we calculated the timelike geodesics, which possess a rich structure and allow different kinds of trajectories for the particles. This work, along with the null geodesic described in Ref. [10], complements the geodesic structure for the rotating three-dimensional Hořava AdS black hole. For direct orbits, we have shown the existence of planetary orbits, where we have obtained an exact

solution and we have determined the periods of revolution. Also, for circular orbits, we have shown the existence of the stable and unstable circular orbits, and we determined the periods of revolution, as well as the epicycle frequency for the stable circular orbit, and also critical orbits of the first and second kind that approach the unstable circular orbit asymptotically. For the motion with $0 \leq L < L_C$, the trajectories are all bounded, and for $L = 0$, we have obtained exact solutions. However, their counterpart, i.e., the BTZ metric, allows geodesics for massive particles that always fall into the event horizon and no stable orbits are possible; thereby, the differences observed with respect to the BTZ metric could be attributed to the breaking of the Lorentz invariance. On the other hand, for retrograde orbits, we have shown the existence of the second kind orbits, similar to the behavior observed for retrograde orbits in a BTZ black hole background [4]. In addition, by comparing both orbits, direct and retrograde, in a rotating three-dimensional Hořava AdS black hole, it is possible to observe trajectories with $E \leq 0$ for retrograde orbits, which is not possible for direct orbits.

Therefore, the Lorentz-violating version of the BTZ black hole turns on an effective potential with a more rich structure, allowing different kinds of orbits. As it was shown [10], for photons new kinds of orbits are allowed, such as unstable circular orbits and trajectories of the first kind. While for particles, the planetary and circular orbits are allowed, which does not occur in the BTZ background. In this way, the breaking of the Lorentz invariance could generate orbits that could not occur in invariant Lorentz theories.

ACKNOWLEDGMENTS

We thank the referee for careful review of the manuscript and valuable comments and suggestions, which helped us to improve the manuscript. Y. V. acknowledges support by the Dirección de Investigación y Desarrollo de la Universidad de La Serena, Grant No. PR18142.

- [1] M. Bañados, C. Teitelboim, and J. Zanelli, The Black Hole in Three-Dimensional Space-Time, *Phys. Rev. Lett.* **69**, 1849 (1992).
- [2] S. Carlip, The $(2 + 1)$ -dimensional black hole, *Classical Quant. Grav.* **12**, 2853 (1995).
- [3] C. Farina, J. Gamboa, and A. J. Segui-Santonja, Motion and trajectories of particles around three-dimensional black holes, *Classical Quant. Grav.* **10**, L193 (1993).
- [4] N. Cruz, C. Martínez, and L. Pena, Geodesic structure of the $(2 + 1)$ black hole, *Classical Quant. Grav.* **11**, 2731 (1994).
- [5] T. P. Sotiriou, M. Visser, and S. Weinfurter, Lower-dimensional Hořava-Lifshitz gravity, *Phys. Rev. D* **83**, 124021 (2011).
- [6] T. P. Sotiriou, I. Vega, and D. Vernieri, Rotating black holes in three-dimensional Hořava gravity, *Phys. Rev. D* **90**, 044046 (2014).
- [7] P. Hořava, Quantum gravity at a Lifshitz point, *Phys. Rev. D* **79**, 084008 (2009).
- [8] R. Bécár, P. A. González, E. Papantonopoulos, and Y. Vásquez, Quasinormal modes of three-dimensional rotating Hořava AdS black hole and the approach to thermal equilibrium, *Eur. Phys. J. C* **80**, 600 (2020).
- [9] R. Bécár, P. A. González, and Y. Vásquez, Collision of particles near a three-dimensional rotating Hořava AdS black hole, *Eur. Phys. J. C* **81**, 252 (2021).
- [10] P. A. González, M. Olivares, E. Papantonopoulos, and Y. Vásquez, Motion and trajectories of photons in a three-dimensional rotating Hořava-AdS black hole, *Phys. Rev. D* **101**, 044018 (2020).
- [11] S. Fernando, D. Krug, and C. Curry, Geodesic structure of static charged black hole solutions in $2 + 1$ dimensions, *Gen. Relativ. Gravit.* **35**, 1243 (2003).
- [12] N. Cruz, M. Olivares, and J. R. Villanueva, Geodesic structure of Lifshitz black holes in $2 + 1$ dimensions, *Eur. Phys. J. C* **73**, 2485 (2013).
- [13] S. Kazempour and S. Soroushfar, Investigation the geodesic motion of three dimensional rotating black holes, *Chin. J. Phys.* **65**, 579 (2020).
- [14] G. Panotopoulos, Orbits of test particles in three-dimensional Maxwell-dilaton spacetime: Exact analytical solution to the geodesic equation, *Gen. Relativ. Gravit.* **52**, 54 (2020).
- [15] T. Jacobson, Extended Hořava gravity and Einstein-aether theory, *Phys. Rev. D* **81**, 101502 (2010); Erratum, *Phys. Rev. D* **82**, 129901 (2010).
- [16] B. Cropp, S. Liberati, A. Mohd, and M. Visser, Ray tracing Einstein-aether black holes: Universal versus killing horizons, *Phys. Rev. D* **89**, 064061 (2014).
- [17] T. Zhu, Q. Wu, M. Jamil, and K. Jusufi, Shadows and deflection angle of charged and slowly rotating black holes in Einstein-aether theory, *Phys. Rev. D* **100**, 044055 (2019).
- [18] S. Chandrasekhar, *The Mathematical Theory of Black Holes* (Oxford University Press, New York, 1983).
- [19] N. Deruelle and R. Ruffini, Quantum and classical relativistic energy states in stationary geometries, *Phys. Lett.* **52B**, 437 (1974).
- [20] In this work, we have considered choosing values for the parameters such that the zeros of terms in square brackets are not located in the relevant domain, they are inside the event horizon.
- [21] J. Ramos-Caro, J. F. Pedraza, and P. S. Letelier, Motion around a monopole + ring system: I. Stability of equatorial circular orbits vs regularity of three-dimensional motion, *Mon. Not. R. Astron. Soc.* **414**, 3105 (2011).